A Tensor-Based Holographic Multi-Feed Antenna Synthesis for MIMO Radar Applications

Thomas Frey*, Jens Österle, Maximilian Döring, Christian Waldschmidt, Tobias Chaloun
*Institute of Microwave Engineering, University Ulm, 89081 Ulm, Germany
Email: thomas.frey@uni-ulm.de

***Abstract*—A novel hologram synthesis method using the full impedance tensor for multi-feed holographic-based leaky wave antennas (HLWAs) is presented. Since, the unit cells (UCs) are shared across all feeds, all sub-holograms need to be combined into a shared holographic aperture. The shared impedance tensor is determined by minimizing the error relative to all sub-tensors for every UC. Based on the full tensorial multi-feed synthesis, a HLWA having two feeding points is fabricated on a fused silica wafer for an operational frequency of 160 GHz. The far field measurements show an antenna gain of 31.0 dBi and 31.4 dBi, corresponding to an aperture efficiency of 35 % and 38 %. The high gain and narrow beam of each feed make the antenna well-suited for an integration into a long-range MIMO radar. A polarization purity of less than 27 dB and a side-lobe level below −20.0 dB were measured at 160 GHz.**

***Index Terms*—Holographic antenna, metasurface antenna, multi-feed antenna, multiple-input multiple-output (MIMO), impedance tensor, surface wave, leaky wave, glass technology.**

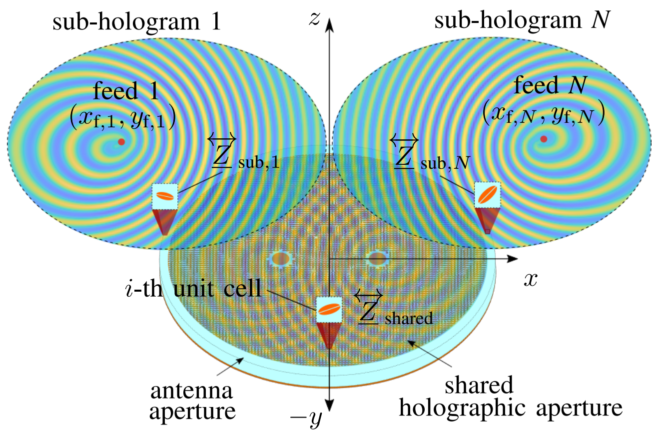

Fig. 1: Generation of a single physical shared holographic aperture across all N sub-holograms.

I. Introduction

Holographic-based leaky wave antennas (HLWAs) allow a highly flexible control of the aperture field in terms of the amplitude as well as phase distribution, and also regarding the polarization of the electromagnetic far field [1], [2]. This can be achieved through the interaction of a surface wave (SW) mode with a periodically modulated impedance surface (MIS). The MIS hologram arises as an interference pattern of a bounded SW mode propagating along an interface between two dissimilar materials and a continuously radiating leaky wave (LW) mode. A dense periodic structure of sub-wavelength discontinuities $\left(\approx \frac{\lambda_0}{10}\right)$ placed on a grounded dielectric slab can be utilized to realize the TM-based MIS hologram.

The HLWA is intended for an integration into a long-range multiple-input multiple-output (MIMO) imaging radar, necessitating several feeding points on the same antenna aperture. However, only the realization of a single pixel geometry within a unit cell (UC) is feasible. To accomplish this, a superposition of all individual sub-holograms with their corresponding pixel geometries into a shared holographic aperture has to be implemented.

In recent works, the superposition is performed by a pixel-based arithmetic averaging of all individual impedance sub-holograms [3]. This physically corresponds to an arithmetic averaging of the individual pixel geometries and results in an increased deviation between the shared holographic aperture and the individual sub-holograms. In [4] the hologram superposition is implemented by taking the UC-related incident angle into account, leading to a more accurate implementation of the shared holographic aperture.

In this paper, a novel full tensorial multi-feed synthesis for HLWAs is presented. Instead of using the scalar impedance for the superposition, the full impedance tensor is employed. This results in an even more accurate realization of the individual sub-holograms through a shared holographic aperture, particularly enhancing the antenna gain, beam symmetry and polarization purity in terms of the improved anisotropy degree [5]. These improvements make the HLWA particularly suitable for a long-range MIMO radar in terms of high range and high resolution. A multi-feed HLWA prototype is fabricated on a fused silica wafer, motivated by the high manufacturing precision achievable with the wet etching process at frequencies above 140 GHz [6].

II. Synthesis Method for Multi-Feed HLWAs

In order to generate a continuously radiating LW mode a bounded SW propagating at an interface between two dissimilar materials is necessary. Therefore, each feeding point excites the fundamental TM_0 SW mode propagating rotationally symmetric on the antenna aperture [7]. Its transverse magnetic field distribution $\underline{\vec{H}}_{\mathrm{t}}|_{z=0^+}$ follows the

Hankel function of the second kind and first order [2]. The MIS hologram consists of surface impedance tensors $\overleftrightarrow{\underline{Z}}$ that link the transverse magnetic field $\underline{\vec{H}}_{\mathrm{t}}$ to the transverse electric field distribution $\underline{\vec{E}}_{\mathrm{t}}$. This is mathematically described through the space-dependent impenetrable impedance boundary condition (IIBC) as [1]

$$\begin{pmatrix} \underline{E}_{\mathrm{t},x} \\ \underline{E}_{\mathrm{t},y} \end{pmatrix} = \begin{pmatrix} \underline{Z}_{xx} & \underline{Z}_{xy} \\ \underline{Z}_{yx} & \underline{Z}_{yy} \end{pmatrix} \cdot \left(\vec{e}_z \times \begin{pmatrix} -\underline{H}_{\mathrm{t},y} \\ \underline{H}_{\mathrm{t},x} \end{pmatrix} \right), \qquad (1)$$

where $\vec{e}_z$ describes the unit vector normal to the antenna aperture. If the anisotropic tensor components $\underline{Z}_{xy}$ or $\underline{Z}_{yx}$ exist, a TM/TE coupling occurs and the fundamental TM_0 SW mode is converted into a radiating TM-TE-hybrid LW mode. The objective aperture field distribution has the following form

$$\underline{\vec{E}}_{\mathrm{obj}}(x,y) = \vec{T}(x,y) \circ \vec{E}_0 \circ \begin{pmatrix} \mathrm{e}^{-\mathrm{j}(k_x x)} \\ \mathrm{e}^{-\mathrm{j}\left(k_y y \mp \frac{\pi}{2}\right)} \end{pmatrix}, \qquad (2)$$

with $\circ$ being the Hadamard product and $\vec{T}(x,y)$ defines the x- and y-components of the desired planar amplitude taper function. An arbitrary polarization is provided by the complex phase term, but in this work a circularly polarized excited electric field is used. The constant space independent field amplitudes are described by $\vec{E}_0$. The synthesis results in an impedance tensor hologram depending on the predefined objective field distribution (2) and the magnetic field of the SW. The interaction between the TM_0 SW mode and the impedance tensor hologram leads to the radiating portion of the transverse electric field $\underline{\vec{E}}_{\mathrm{t},(-1,-1)}$ corresponding to the electric field distribution of the $(-1,-1)$-LW mode.

The design of a HLWA having N multiple feeding points involves synthesizing the impedance hologram for each individual feed n located at $(x_{\mathrm{f},n},\, y_{\mathrm{f},n})$ on the antenna aperture (see Fig. 1). This results in N impedance tensor sub-holograms $\mathscr{H}_{\mathrm{sub},n}$, whose origin corresponds to their feeding position

$$\mathscr{H}_{\mathrm{sub},n}(x_{\mathrm{f},n},\, y_{\mathrm{f},n}) \quad \forall\, n \in \mathbb{N}. \qquad (3)$$

Each individual sub-hologram is discretized into a periodic arrangement of I UCs, where each i-th UC of a sub-hologram represents an impedance tensor

$$\overleftrightarrow{\underline{Z}}_{\mathrm{sub},n}(x_{\mathrm{uc},i}, y_{\mathrm{uc},i}) \quad \forall\, n \wedge i \in \mathbb{N}, \qquad (4)$$

as shown in Fig. 1. The impedance tensor $\overleftrightarrow{\underline{Z}}_{\mathrm{sub},n}$ from each sub-hologram can be represented by a pixel geometry within a UC. However, only a single physical realization of the impedance hologram on the antenna aperture is possible. Thus, a shared holographic aperture $\mathscr{H}_{\mathrm{shared}}$ is established with a shared impedance tensor $\overleftrightarrow{\underline{Z}}_{\mathrm{shared}}(x_{\mathrm{uc},i}, y_{\mathrm{uc},i})$ for each UC across all N sub-holograms, as illustrated in Fig. 1.

A. Angular-Dependent Hologram Superposition

For the sake of comparison, the state-of-the-art approach for multi-feed HLWA designs is briefly introduced. The superposition of all individual sub-holograms into a shared holographic aperture is implemented by taking into account the UC-related angle of incidence [4]. The minimum impedance error $\vec{e}$ between all N angular-dependent scalar impedances $\underline{Z}_{s,\mathrm{sub},n}$ and the 2-D-look-up table (LUT) $\underline{Z}_{s,\mathrm{LUT}}$

$$\vec{e}(w_{\mathrm{pxl},m}) = \sum_{n=1}^{N} \Big| \underline{Z}_{s,\mathrm{LUT}}(\phi_{\mathrm{pxl,shared}} + \phi_{\mathrm{inc},n}, w_{\mathrm{pxl},m}) - \underline{Z}_{s,\mathrm{sub},n} \Big| \qquad (5)$$

determines the shared pixel geometry $(\phi_{\mathrm{pxl,shared}},\, w_{\mathrm{pxl,shared}})$ and the corresponding angular-dependent scalar impedances $\underline{Z}_{s,\mathrm{shared},n}(\phi_{\mathrm{pxl,shared}} + \phi_{\mathrm{inc},n},\, w_{\mathrm{pxl,shared}})$. This angular-dependent superposition (ADS) method is performed for every i-th UC on the antenna aperture. The interested reader is referred to [4]. This design methodology takes the UC-related incidence angle ϕ_{inc} into account, but the mapping of the analytical tensor to the corresponding pixel geometry parameters is performed by using the scalar impedance. The deviation of the shared holographic aperture $\mathscr{H}_{\mathrm{shared}}$ to each n-th sub-hologram $\mathscr{H}_{\mathrm{sub},n}$ leads to an absolute hologram error

$$\mathscr{H}_{\mathrm{error}} = \sum_{n=1}^{N} \big| \mathscr{H}_{\mathrm{sub},n} - \mathscr{H}_{\mathrm{shared}} \big|. \qquad (6)$$

The hologram error directly affects the synthesized objective aperture field distribution of the shared holographic aperture due to the IIBC (1). Consequently, an increased deviation of the synthesized radiation patterns from the ideal radiation patterns, which originate from the ideal sub-holograms can be observed.

B. Full Tensorial Hologram Superposition

To overcome the drawback of the ADS approach (Sec. II-A), a full tensorial superposition (FTS) method for multi-feed HLWAs is presented. For a more accurate combination of all sub-holograms into a shared holographic aperture, all impedance tensor components are taken into account. This ensures a more precise implementation of the analytical sub-tensors $\overleftrightarrow{\underline{Z}}_{\mathrm{sub},n}$ and minimizes the impedance error to the shared tensor $\overleftrightarrow{\underline{Z}}_{\mathrm{shared}}$.The individual pixel orientation angles $\phi_{\mathrm{pxl},n}$ of the analytical sub-tensors are computed using the eigenvector (EV) approach from [4]. This results in $N \times M \times 4$ tensor 3D LUT $\overleftrightarrow{\underline{Z}}_{\mathrm{LUT}}$ consisting of N rows defined by the pixel orientation angles, M columns for the different pixel widths $w_{\mathrm{pxl},m}$ and the four tensor components

$$\overleftrightarrow{\underline{Z}}_{\mathrm{LUT}}(\phi_{\mathrm{pxl},n}, w_{\mathrm{pxl},m}) \quad \forall\, m \wedge n \in \mathbb{N}. \qquad (7)$$

Subsequently, the UC-referred incident angle $\phi_{\mathrm{inc},n}$ of each feed is added to the corresponding pixel orientation $\phi_{\mathrm{pxl},n}$. The orientation of the shared pixel $\phi_{\mathrm{pxl,shared}}$ is computed under the condition of minimizing the relative error to all the individual angles $\phi_{\mathrm{pxl},n}$ for each UC. The goal is to minimize the tensor error $\overleftrightarrow{e}$ across all individual sub-tensors in comparison to the LUT tensor, in order to determine the shared pixel width $w_{\text{pxl,shared}}$ for each UC

$$\overleftrightarrow{e}(w_{\text{pxl},m}) = \sum_{n=1}^{N} \Big| \overleftrightarrow{\underline{Z}}_{\text{LUT}}(\phi_{\text{pxl,shared}}, w_{\text{pxl},m}) - \overleftrightarrow{\underline{Z}}_{\text{sub},n} \Big| . \tag{8}$$

The error vector $\vec{e}$ is calculated using the 1-Norm $\|\cdot\|_1$ of the error tensor (8) as a function of the pixel width w_{pxl}. Subsequently, the shared pixel width is determined by the column with the lowest impedance error value

$$w_{\text{pxl,shared}} = \underset{w_{\text{pxl},m}}{\operatorname{argmin}} \Big\{ \vec{e}(w_{\text{pxl},m}) \Big\} . \tag{9}$$

The corresponding shared impedance tensor $\overleftrightarrow{\underline{Z}}_{\text{shared}}$ is determined from the 3D-tensor LUT $\overleftrightarrow{\underline{Z}}_{\text{LUT}}$ using the shared pixel geometry

$$\overleftrightarrow{\underline{Z}}_{\text{shared}} = \overleftrightarrow{\underline{Z}}_{\text{LUT}}(\phi_{\text{pxl,shared}}, w_{\text{pxl,shared}}) . \tag{10}$$

Instead of achieving the superposition of all sub-holograms by a pixel-wise arithmetic averaging [3], the presented FTS method determines the shared tensor $\overleftrightarrow{\underline{Z}}_{\text{shared}}$ and its corresponding pixel geometry parameters under the condition of minimizing the error relative to all N analytical sub-tensors. The FTS process is performed for each i-UC on the antenna aperture for the realization of the analytical sub-holograms as a shared holographic aperture (see Fig. 1).

C. Error and Performance Evaluation

In order to evaluate the improvement of the novel FTS method (Sec. II-B) compared to the ADS approach (Sec. II-A), the root meas square (RMS) error of the dispersion curve over the whole tensor hologram $e_{\text{D,RMS,Holo},n}$ is utilized for each n-th feeding point [8]

$$e_{\text{D,RMS,Holo},n} = \sqrt{\frac{1}{PI} \sum_{i=1}^{I} \sum_{p=0}^{P} |e_{\text{D},p}|^2} \;\forall p \in [0, 360] \wedge \forall i \in \mathbb{N} . \tag{11}$$

The error $e_{\text{D,RMS,Holo},n}$ describes the misalignment between the dispersion curves of the N analytical impedance tensors from the sub-holograms $\overleftrightarrow{\underline{Z}}_{\text{sub},n}$ and the shared tensor $\overleftrightarrow{\underline{Z}}_{\text{shared}}$ across all I UCs on the antenna aperture.

The aperture efficiency (AE) is a key parameter in the antenna design and is used to evaluate the multi-feed hologram synthesis. With respect to each n-th feeding point on the antenna aperture and its corresponding radiating beam, the aperture efficiency per feed $\eta_{\text{A},n}$ is calculated as follows

$$\eta_{\text{A},n} = N \frac{\lambda_0^2 \, G_{\text{meas},n}}{4\pi \, A_{\text{geom}}} , \tag{12}$$

where λ_0 is the free-space wavelength, A_{geom} equals the physical aperture area, the number of feeding points is defined by N and $G_{\text{meas},n}$ corresponds to the measured antenna gain for each feeding point.

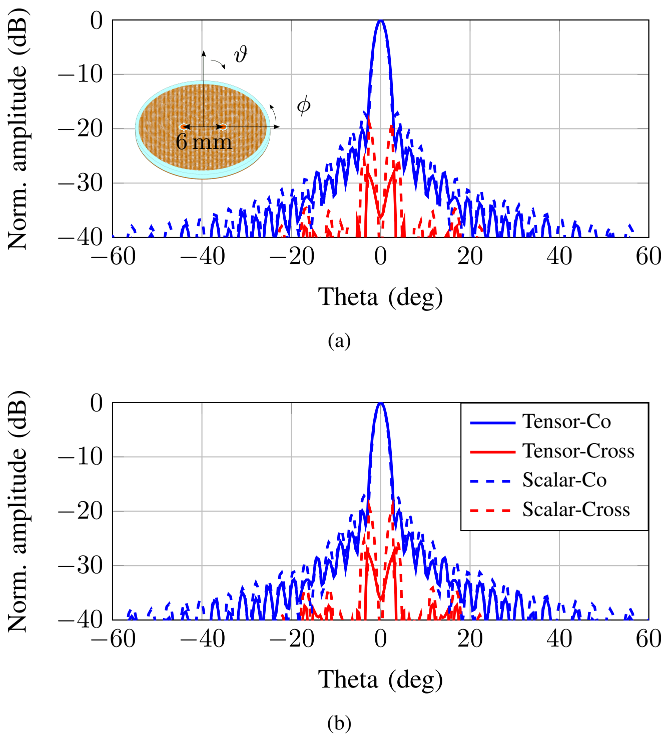

Fig. 2: Comparison of the analytical radiation pattern for the two feeds at $x_{\text{f},1,2} = \pm 3\,\text{mm}$, $y_{\text{f},1,2} = 0\,\text{mm}$ using the ADS approach (dashed line) and FTS method (solid line) at $160\,\text{GHz}$. (a) Feed 1 at $\phi_0 = 0°$. (b) Feed 2 at $\phi_0 = 0°$.

III. HLWA Design Process and Analytical Comparison

Based on the novel full tensorial multi-feed synthesis method discussed in Sec. II, a HLWA prototype is designed on a fused silica wafer. In order to suppress higher order SW modes, the thickness of the glass wafer was chosen to $160\,\mu\text{m}$. The HLWA has two feeds located at ($x_{\text{f},1} = -3\,\text{mm}$, $y_{\text{f},1} = 0\,\text{mm}$) and ($x_{\text{f},2} = 3\,\text{mm}$, $y_{\text{f},2} = 0\,\text{mm}$) and is designed for an operational frequency of $160\,\text{GHz}$. Two coplanar waveguides (CPWs) within the ground metallization are used to feed the surface wave launcher (SWL) from the bottom side. The CPW dimensions correspond to the characteristic impedance of $50\,\Omega$. The antenna consists of 52900 square UCs and the UC size is set to $0.2\,\text{mm} \times 0.2\,\text{mm}$ in order to ensure a homogeneous periodic structure. This results in an aperture area of $21.16\,\text{cm}^2$. In order to obtain a high degree of anisotropy, the pixel geometry is based on an elliptically shaped metal patch with inclined slot to realize anisotropic impedance tensors. The orientation of the ellipse and the slot is calculated by the eigenvectors of the impedance tensor [4]. These UC dimensions and pixel geometry provide a maximum modulation index of $\max(M_{\text{t}}) = 0.28$ and an average impedance of $\underline{Z}_{\text{avg}} = \text{j}256\,\Omega$. The HLWA is intended to radiate a right-hand circularly polarized (RHCP) pencil beam for each feed in azimuth direction $\phi_{0,1/2} = 0°$ and in elevation angle of $\vartheta_{0,1/2} = 0°$ at $160\,\text{GHz}$. The co-polarization

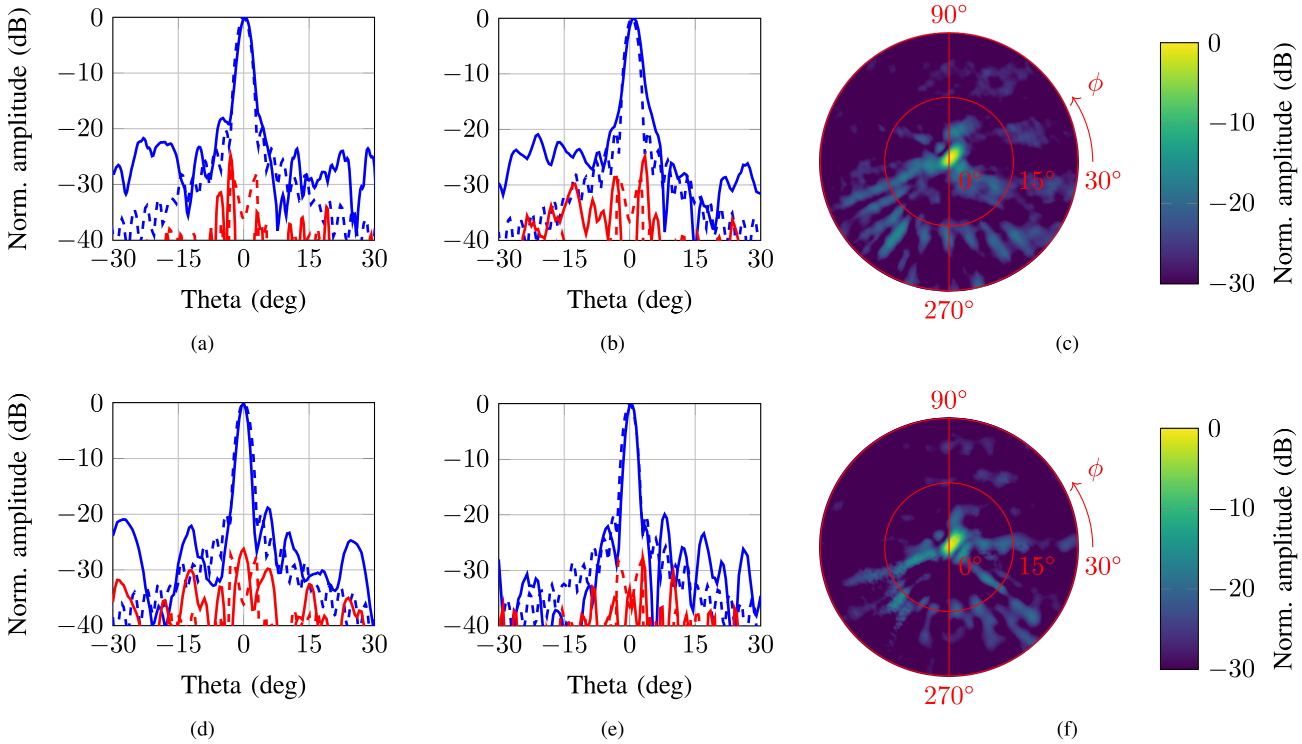

Fig. 3: Measured (solid) and IIBC computed (dashed) radiation pattern of each feeding point of the multi-feed HLWA having two feeds at an operational frequency of 160 GHz. Co-pol (—) and cross-pol (—). (a) - (c) Feed 1: (a) $\phi_0 = 0°$, (b) $\phi_0 = 90°$ and (c) measured 3D-radiation pattern. (d) - (f) Feed 2: (d) $\phi_0 = 0°$, (e) $\phi_0 = 90°$ and (f) measured 3D-radiation pattern.

and cross-polarization of the IIBC computed radiation patterns resulting from the ADS approach (Sec. II-A) and the novel FTS method (Sec. II-B) for both feeding points are depicted in Fig. 2. The radiation pattern based on the FTS method provide a significant improvement of the side-lobe level (SLL) by 5 dB and an increase in polarization purity of 8 dB (see Fig. 2). This results from the significant reduction of the RMS error of the dispersion curve $e_{\text{D,RMS,Holo}}$ (11) over the whole tensor hologram of 43 % from 56.8 Ω to 32.4 Ω. This leads to a more accurate implementation of the shared holographic aperture in comparison to the ADS method and yields an improvement in antenna gain of at least 1.15 dB.

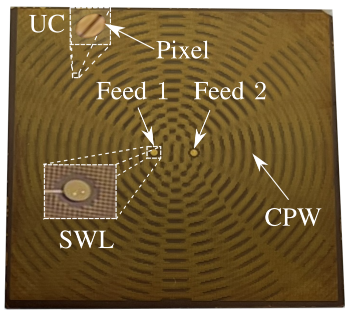

Fig. 4: Top view photography of the manufactured multi-feed HLWA prototype on glass technology.

IV. HLWA Realization and Measurements

The anisotropic HLWA prototype on glass, based on the full tensorial multi-feed synthesis method (Sec. II-B), was fabricated on a fused silica wafer with a relative permittivity $\varepsilon_r = 3.78$ and a dielectric loss factor $\tan\delta = 0.001$. The metallization for the periodic pixel structures and the ground plane consists of a 10 nm thick chromium seed layer, to which a 350 nm thick gold layer is added. The individual pixel structures are realized by a conventional wet etching process with tolerances of ±2 µm. A probe tip in upside-down orientation is used to feed the proposed HLWA on glass from the bottom side in order to avoid the parasitic effect of the probe on the radiation pattern of the antenna under test (AUT). The similar measurement setup was applied as described in [7]. The manufactured multi-feed HLWA prototype on glass technology is depicted in Fig. 4. The far field measurements are conducted using a robot-supported mm-wave antenna measurement setup [9]. In Fig. 3 the measured radiation patterns for feed 1 (Fig. 3a - 3c) and feed 2 (Fig. 3d - 3f) of the multi-feed HLWA are illustrated for an elevation angles in the range ±30° at the azimuth angles 0° (Fig. 3a & 3d) and 90° (Fig. 3b & 3e) all at 160 GHz. A minimum SLL of −19 dB and −20 dB and a polarization purity below 27 dB were measured. The co-polarization component of the measured 3D radiation patterns are shown in Fig. 3c & 3f

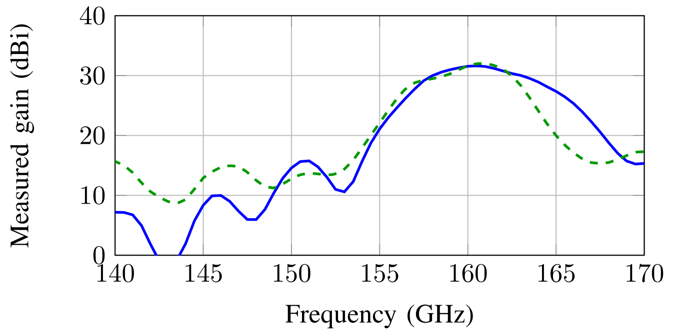

Fig. 5: Measured antenna gain vs. frequency from 140 GHz to 170 GHz of the realized multi-feed HLWA prototype on glass. (Feed 1 (—), feed 2 (- - -)).

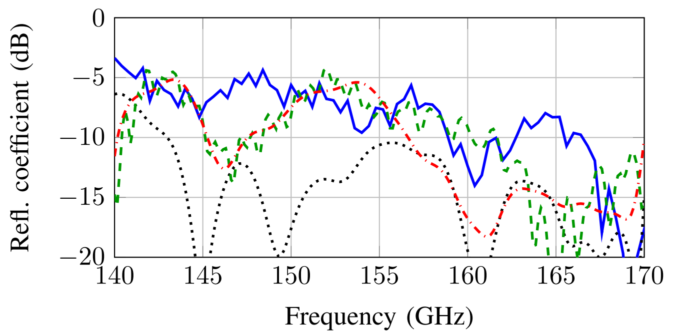

Fig. 6: Measured input reflection coefficient vs. frequency from 140 GHz to 170 GHz of the realized multi-feed HLWA prototype on glass. (Feed 1: (—) original data, (···) data w/o probe tips, feed 2: (- - -) original data, (- - -) w/o probe tips).

for elevation angles up to $\pm30°$ and for all azimuth angles. For both feeds, the shape of the main beam, the SLL, and the polarization purity are very well-defined in all azimuth planes. Overall, the radiation patterns show an excellent agreement between the measured and simulated results. The measured antenna gain across a wide frequency range from 140 GHz to 170 GHz is shown in Fig. 5. A measured gain for feed 1 and feed 2 of 31 dBi and 31.4 dBi, respectively, can be determined (see Fig. 5), resulting in an aperture efficiency for each individual feeding point (12) of $\eta_{A,1} = 35\,\%$ and $\eta_{A,2} = 38\,\%$. This corresponds to an improvement of at least 1.1 dB compared to the ADS synthesis of Sec. II-A. Furthermore, a gain imbalance of 0.4 dB is achieved at the operational frequency of 160 GHz. The computed directivity based on the 3D radiation patterns are 31.7 dBi and 32.1 dBi, respectively, which corresponds to a minimum radiation efficiency of 85 %. The high-directive and narrow pencil beam characteristic results in an extended range and enhanced resolution for long-range MIMO radar applications. The input reflection coefficient for both feeds is illustrated in Fig. 6 across a bandwidth of 30 GHz from 140 GHz to 170 GHz. Additionally, the probe tip and spurious reflections from the environment have been removed by means of time domain filtering, resulting in reflection coefficients of −17 dB and −19 dB for both feeds at 160 GHz.

V. Conclusion

In this paper, a novel hologram synthesis method using the full impedance tensor for multi-feed holographic-based leaky wave antennas is presented. A tensorial shared holographic aperture is determined, which has the lowest impedance error to the corresponding analytical sub-holograms. The antenna has been designed with two feeding points towards a long-range MIMO imaging radar application. The spherical radiation characteristics of the multi-feed HLWA have been validated up to elevation angles of $\pm30°$ and for the whole azimuth plane. The measured radiation patterns show an antenna gain of 31 dBi and 31.4 dBi, respectively, corresponding to an notable AE of 35 % and 38 %. A side-lobe level of at least −19 dB, and a minimum polarization purity of 27 dB were measured at an operation frequency of 160 GHz.

Acknowledgment

This work was funded by the Deutsche Forschungsgemeinschaft (DFG, German Research Foundation) – CH 2226/4-1. The authors would like to thank to Norbert Ambrosius from LPKF Laser & Electronics AG for processing and machining the glass wafer, Stefan Jenisch from the Institute for Electronic Components and Circuits at Ulm University and Heike Frik from the Institute of Microwave Engineering at Ulm University for their technical support in realizing the HLWA Prototype on glass.

References

[1] G. Minatti, F. Caminita, M. Casaletti, and S. Maci, "Spiral Leaky-Wave Antennas Based on Modulated Surface Impedance," *IEEE Trans. Antennas Propag.*, vol. 59, no. 12, pp. 4436–4444, Dec. 2011.

[2] G. Minatti, M. Faenzi, E. Martini, F. Caminita, P. D. Vita, D. González-Ovejero, M. Sabbadini, and S. Maci, "Modulated Metasurface Antennas for Space: Synthesis, Analysis and Realizations," *IEEE Trans. Antennas Propag.*, vol. 63, no. 4, pp. 1288–1300, Apr. 2015.

[3] M. Faenzi, D. González-Ovejero, G. Petraglia, G. D Alterio, F. Pascariello, R. Vitiello, and S. Maci, "A Metasurface Radar Monopulse Antenna," *IEEE Trans. Antennas Propag.*, vol. 70, no. 4, pp. 2571–2579, 2022.

[4] T. Frey, M. Döring, N. Riese, C. Waldschmidt, and T. Chaloun, "Angle-Dependent Synthesis Method for Holographic Multi-Feed Antennas," *IEEE Open Journal of Antennas and Propagation*, vol. 4, pp. 392–407, 2023.

[5] T. Frey, M. Döring, C. Waldschmidt, and T. Chaloun, "A Full Tensorial Synthesis Method for Holographic-Based Leaky Wave Antennas," *IEEE Antennas Wireless Propag. Lett.*, pp. 1–5, 2023.

[6] T. Chaloun, S. Brandl, N. Ambrosius, K. Kröhnert, H. Maune, and C. Waldschmidt, "RF Glass Technology Is Going Mainstream: Review and Future Applications," *IEEE Journal of Microwaves*, vol. 3, no. 2, pp. 783–799, 2023.

[7] T. Galler, T. Frey, C. Waldschmidt, and T. Chaloun, "High-Gain Millimeter-Wave Holographic Antenna in Package using Glass Technology," *IEEE Antennas Wireless Propag. Lett.*, pp. 1–5, 2020.

[8] T. Frey, M. Döring, C. Waldschmidt, and T. Chaloun, "An Eigenvector-Supported Optimization Method for Holographic-Based Leaky Wave Antennas," in *2024 18th European Conference on Antennas and Propagation (EuCAP)*, 2024, pp. 1–5.

[9] L. Boehm, F. Boegelsack, M. Hitzler, and C. Waldschmidt, "The Challenges of Measuring Integrated Antennas at Millimeter-Wave Frequencies," *IEEE Antennas Propag. Mag.*, vol. 59, no. 4, pp. 84–92, Aug. 2017.